Autonomous Wristband Placement in a Moving Hand for Victims in Search and Rescue Scenarios With a Mobile Manipulator

Francisco Pastor[1], Francisco J. Ruiz-Ruiz[1], Jesús M. Gómez-de-Gabriel[1], *Member, IEEE*,
Alfonso J. García-Cerezo[1], *Senior Member, IEEE*

Abstract— In this letter, we present an autonomous method for the placement of a sensorized wristband to victims in a Search-And-Rescue (SAR) scenario. For this purpose, an all-terrain mobile robot includes a mobile manipulator, which End-Effector (EE) is equipped with a detachable sensorized wristband. The wristband consists of two links with a shared shaft and a spring. This configuration allows the wristband to maintain fixed to the EE while moving and get placed around the victim's forearm once the contact is produced. The method has two differentiated phases: i) The visual moving hand tracking phase, where a 3D vision system detects the victim's hand pose. At the same time, the robotic manipulator tracks it with a Model Predictive Controller (MPC). ii) The haptic force-controlled phase, where the wristband gets placed around the victim's forearm controlling the forces exerted. The wristband design is also discussed, considering the magnitude of the force needed for the attachment and the torque the wristband exerts to the forearm. Two experiments are carried out, one in the laboratory to evaluate the performance of the method and the second one in a SAR scenario, with the robotic manipulator integrated with the all-terrain mobile robot. Results show a 97.4% success in the wristband placement procedure and a good performance of the whole system in a large scale disaster exercise.

I. INTRODUCTION

Between 2005 and 2014, almost a million people lost their lives in artificial disaster scenarios, such as terrorist events or industrial accidents, and in natural disaster scenarios, such as earthquakes, wildfires or meteorological disasters [1]. When a disaster strikes, a rapid and coordinated response of the rescue teams is crucial, reducing the number of victims and mitigating the economic impact [2]. The most common response is to rescue victims and transport them to hospitals. In large scale disaster scenarios, performing a good triage is crucial to saving the maximum amount of lives, as hospitals may collapse [3].

Most of the existing works to provide safe triage and continuous monitoring are based on the placement of remote biomedical sensors that offer remote monitoring of the victim's localization and status [4], [5]. Biomedical sensors have also proved their effectiveness in Search And Rescue (SAR) scenarios, recording stress-related parameters in a rescue human operator [6]. Sensorized wristbands have some key advantages, such as their portability and ubiquity, allowing
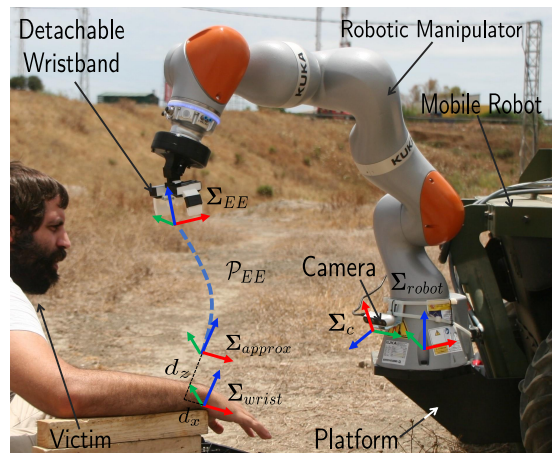
Fig. 1. The autonomous wristband placement method with the robotic manipulator installed in a mobile robot in a SAR operation. The XYZ-RGB convention is used in this figure.

a safe interaction when getting placed and avoiding contact with vital organs. These devices can also provide real-time continuous wireless information [7], [8].

Robots in disaster scenarios are frequently utilized, considering their assistance has been widely proven to be beneficial for the development of these interventions [9]. In several cases, the aid of the victims may be dangerous [10], as there might be high-risk conditions such as radioactive environments, collapsed buildings, or gas leaks taking place. Robots are also capable of exploring unknown environments [11] and tracking human bodies through multiple drones in outdoor environments [12]. In [13], a drone can locate victims in a SAR scenario by recognizing wireless devices with depleted batteries, such as mobile phones, by making them active through wireless power transfer.

Although the use of robotics in SAR, in most cases, involves some contact between the human and the robots, there are still minimal works that study the physical Human-Robot Interaction (pHRI) needed to perform the triage or the placement of sensing devices. In the event of an unconscious victim, his hand may not be suitable for the sensor placement; therefore, further interaction is needed to relocate the body parts (e.g. upper-limbs), so the sensor device can be properly installed. In [14], the first approach to human-limb manipulation is presented, with a robotic manipulator grasping a victim's forearm and estimating its roll angle for precise placement and safe manipulation. However, the approximation to the victim is not addressed, and the initial
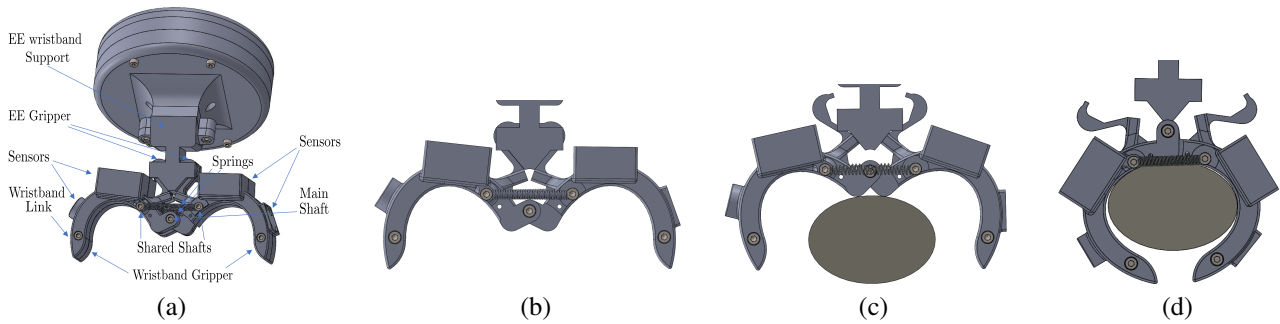
Fig. 2. The complete design of the wristband is presented in (a). In (b), the state I is shown, being the wristband fixed to the manipulator EE. In (c), state II is presented, with the wristband in a singular configuration, while in (d), the wristband is in state III, placed around the victim's wrist.

location of the wrist is supposed to be known.

In [15], an aerial-robot-based solution to deliver remote sensors to the victims using a lightweight delta manipulator has been developed, with a 67.99 % hand detection accuracy. Nevertheless, aerial manipulation solutions require minimum weather conditions, and the accuracy may not be high enough to be a stable solution.

Although robotics has improved the rescue response considerably, there are still no robust robotic solutions for sensing multiple victims once they have been located to obtain their health status and perform continuous triage. This letter presents a novel system for autonomous wristband placement in real disaster scenarios. An all-terrain mobile robot is equipped with a robotic manipulator which integrates a detachable wristband with embedded sensors. Using vision-based methods, the manipulator autonomously tracks a moving hand of a victim and is capable of safely interact with the human to place the wristband in an established position of the victim's forearm. Sensors embedded in the wristband monitor the human's vital signs and tracks his position.

The main contributions of this work are:

- Design of a detachable sensorized wristband and analysis of the forces and torques exerted.
- Definition of an autonomous method to track a moving hand with a robotic manipulator and to place the wristband around the forearm by a haptic force-controlled procedure.
- Evaluation and integration of the proposed method with two experiments carried out in standard conditions and in a SAR scenario as a part of a large scale disaster exercise.

II. RELATED WORKS

A. Hand Tracking Systems

Visual tracking of articulated systems, such as objects [16], human bodies [17], and hands [18], is an active area of research in computer vision. Regarding hand tracking, several studies have been carried out. These studies can be usually separated into model-driven and data-driven approaches [19]. Model-driven methods obtain hand landmarks by comparing a 3D hand model to the image received from the vision sensor. The advantage of driven-based methods is

that the different anatomical size and motion constraints of a human hand are implicitly obtained in the training phase, while data-driven methods need that information to be previously specified. Recent data-driven studies are increasing the robustness and are able to perform in real-time in non-demanding hardware devices [20], [21]. In [20], a single depth image is analyzed from different projections to fully utilize the depth information. In [21], the hand landmarks are obtained from a single RGB image by first recognizing the palm via an oriented hand bounding box and then a hand landmark model that returns 2.5D hand landmarks. These hand tracking solutions provide hand skeleton landmarks, but they lack in giving the palm pose.

There are a few works which provides hand pose estimation. In [22], the posture of a human hand is tracked applying a Kalman and a particle filter to the information provided by a Leap Motion device. Furthermore, in [23], a fusion approach is considered to enhance the performance of the hand pose estimation provided by two Leap Motions. However, these methods have limited workspace and are only suitable for indoor conditions due to the vision sensor they work with.

III. SYSTEM OVERVIEW

A. Detachable Wristband

A sensorized wristband is needed for victim monitoring. The wristband must stay fixed to the EE of the manipulator when it is in motion, and whenever contact with the human is produced, the wristband must get placed around the human forearm. In order to achieve these requirements, a novel passive wristband has been designed. The mechanism consists of two semi-circular wristband links connected by a main shaft and two springs symmetrically placed in two shared shafts that link the system, as seen in Fig. 2 (a). The wristband also has two grips: EE gripper and wristband gripper. With this configuration, three possible states are obtained. State I is shown in Fig. 2 (b). This state is stable, as the springs maintain the EE gripper in contact with the EE wristband support by embracing it, ensuring the wristband remains fixed when the manipulator is moved. State II is a singular configuration, and appears when the two spring shafts and the main shaft are aligned (Fig. 2 (c)). In this
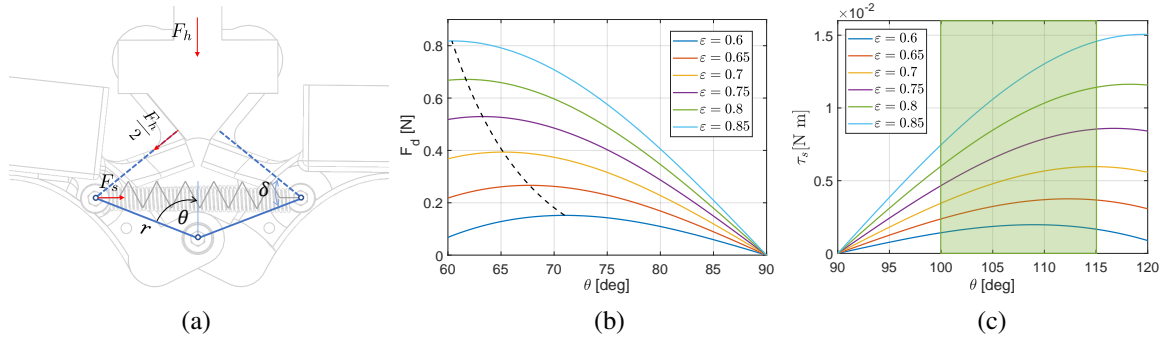
Fig. 3. The schematics of the detachable wristband mechanism are presented in (a). In (b), the detachable force with respect to the θ angle for each value of the parameter ε are represented in a continuous line, while θ_0 and the maximum F_d with respect to the ε are represented in a striped line. In (c), the torque applied by the spring with respect to the θ angle for each value of ε is presented, with, in green, the range of the θ angle for a standard forearm.

position, any differential torque exerted to the main shaft conduct to state I or III, depending on the direction of the torque applied. State III is shown in Fig. 2 (d). In this position, the wristband gripper is in contact with the human arm and remains stable due to the force applied by the springs.

The proposed detachable wristband is also designed to carry different sensors (Fig.2 (a)): Healthcare devices, positioning systems, and communication equipment. Some of these devices must be allocated in specific parts of the forearm in order to operate properly. For instance, some health care sensors obtain better lectures when they are in contact with the anterior forearm due to the tendency to have less hair.

Once the wristband touches the forearm, an interaction force (F_h) is produced. As seen in Fig. 3 (a), this force is assumed to be perpendicular to the main shaft. The transition between state I and state III is produced when the torque applied by F_h to the main shaft is higher than the torque applied by the springs. Therefore, at least a minimum force must be exerted for the wristband to detach. We define the detachable force F_d as the minimum F_h that detaches the wristband from the EE. Hence, F_d produces the same torque in the main shaft as the torque produced by the spring's force (eq.(1)):

$$F_d = 4K_s \frac{\cos(\theta)}{\sin(\delta)}(r\sin(\theta) - \frac{x_0}{2}) \tag{1}$$

where, as seen in Fig. 3 (a), δ is the angle formed by the EE gripper and a wristband link, r is the distance between the main shaft and a shared shaft, x_0 is the spring length in its relaxed position, K_s is the elastic constant of the springs, and θ is the aperture angle between the wristband links divided by two.

A parametric study has been performed to analyze how the detachable force F_d evolves with respect to the θ angle. In Fig. 3 (b), the results of the study are presented with seven values of the parameterization $\varepsilon = \frac{r}{x_0}$, with $\varepsilon = \{0.6 - 0.85\}$, considering null frictional forces and all other parameters are constant. We will define θ_0 as the value of θ when the wristband is attached to the EE wristband support. Considering that the wristband has to remain fixed in the state

I, it is intuitive to conclude that F_d must be at its highest in θ_0. Therefore, a function to obtain in which θ_0 the maximum F_d is produced with respect to the ε parameter has been obtained, deriving eq. (1) with respect to θ and equalizing it to zero:

$$\theta_0 = \text{asin}\left(\frac{\sqrt{32\,\varepsilon^2 + 1} + 1}{8\,\varepsilon}\right). \tag{2}$$

Once θ_0 is known, the maximum F_d can be obtained with eq. (1), and it is represented in Fig. 3 (b) for ε from 0.6 to 0.85.

The torque (τ_s) the wristband links exert to the forearm once it is placed has also been considered in the wristband design. In this case, the wristband is attached to the human forearm and disconnected from the EE ($F_h = 0$). Thus, the torque in the main shaft is due to the force produced by the springs, i.e.,

$$\tau_s = 2\,K_s\,r\cos(\theta)\,\left(r\,\sin(\theta) - \frac{x_0}{2}\right). \tag{3}$$

Another parametric study has been carried out, but this time, analyzing τ_s with respect to θ angle. In Fig. 3 (c), the results are presented with seven values of ε, with $\varepsilon = \{0.6 - 0.85\}$. We will define as θ_f the θ angle when the wristband is in contact with the forearm and remains placed. In green, the range of θ_f for a standard forearm is delimited, being this range $\theta_f = \{100° - 115°\}$. τ_s maintains the wristband fixed, preventing any slippage between the surface of the wristband and the forearm's skin. A compromise must be achieved with the τ_s exerted in the range of θ_f for the ε selected, taking into account that a high torque could harm the victim and a low torque could lead to the wristband releasing from the forearm.

B. All-Terrain Mobile Manipulator with a 3D Vision Sensor

A tele-operated mobile robot is needed for the approximation to the victim in SAR scenarios. Some issues must be addressed for the mobile robot selection. These environments are very demanding, as the path may damage the mobile robot or cause it to lose its stability, making it fall over. Furthermore, it also needs a sufficient payload to carry with the robotic manipulator and all the other electronic components. A robotic manipulator with $n_q \geq 6$ joints is
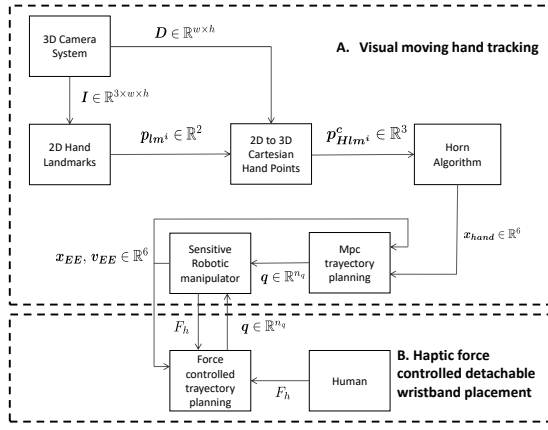
Fig. 4. Schematics of the method, divided in two: A. The hand pose detection process and the MPC trajectory planer of the manipulator and B. the haptic force-controlled linear movement for the wristband placement.

needed since it must be capable of positioning and orientating its EE. The EE frame pose (x_{EE}) can be obtained with $x_{EE} = \mathbb{F}(q)$, where $\mathbb{F}$ is the manipulator forward kinematics function, and q is the joint position vector ($q \in \mathbb{R}^{n_q}$). The velocity of the EE can be computed as $v_{EE} = J(q)\dot{q}$, where J is the Jacobian matrix, and $\dot{q}$ is the joint velocity vector ($\dot{q} \in \mathbb{R}^{n_q}$). The robotic manipulator needs to sense external forces applied in its EE and a workspace large enough to reach a victim lying on the ground. The base frame of the whole system is defined as robot frame ($\sum_{robot}$), and is attached to the base of the manipulator, as seen in Fig. 1.

A 3D vision system is utilized to obtain information about the victim's hand location. The sensor is placed in the base of the robotic manipulator, covering its workspace. A new frame, the camera frame ($\sum_c$) is defined with the origin located in the center of the camera optical and the z_c axis aligned with the optical axis. The camera is calibrated with respect to the robot frame. Since the camera is in eye to hand configuration, the transformation matrix between both frames ($\mathbf{T}_c^{robot}$) is constant.

IV. PROPOSED METHOD

The main aspects of the method are presented, considering the mobile robot has been tele-operated to the victim's location, ensuring the wrist is within the manipulator's workspace. Firstly, the 3D vision system and the control strategy necessary for the moving hand tracking phase are discussed in section IV-A and, then the haptic force-controlled sensorized wristband placement is presented in section IV-B. The whole schematic of the method is shown in Fig. 4.

A. Visual Moving Hand Tracking

The 3D visual tracking problem of a moving hand is considered. For this purpose, the 3D vision system detects the wrist position and the palm orientation, defined as hand pose ($x_{hand} \in \mathbb{R}^6$). Two new frames are also defined (Fig. 1): The wrist frame ($\sum_{wrist}$) and the approximation frame ($\sum_{approx}$). The wrist frame is defined by setting the z_{wrist}

axis perpendicular to the imaginary plane formed by the palm of the hand and the x_{wrist} axis parallel to the forearm. The wrist frame pose with respect to the robot frame is defined coincident with the hand pose, hence $x_{hand} = x_{wrist} = [O_{wrist}, \varphi_{wrist}]$, being $O_{wrist} \in \mathbb{R}^3$ and $\varphi_{wrist} \in \mathbb{R}^3$ the position and orientation wrist frame vectors, respectively. The approximation frame coincides with the wrist frame, but with an offset in the x_{wrist} and z_{wrist} axes, defined as $d = [d_x, 0, d_z]$, being d_x an approximate distance between a palm and a wrist and d_z is a security distance from the End Effector (EE) to the dorsum of a forearm. The transformation matrix between both frames is defined as:

$$\mathbf{T}_{wrist}^{approx} = \begin{bmatrix} \mathbb{I}_{3\times3} & d \\ O_{1\times3} & 1 \end{bmatrix} \quad (4)$$

To define the palm surface, which approximates to a plane, a minimum of 3 non-collinear hand landmarks are necessary, and one must be positioned in the middle of the wrist.

Let us define as two dimensional points (2D) the hand landmarks ($p_{lm^i} = [x_{lm^i}, y_{lm^i}]$, where $i = 1 : n_i$, with $n_i \geq 3$). The points are measured in pixels and are obtained from an RGB image with $w \times h$ resolution ($I \in \mathbb{R}^{3 \times w \times h}$). Let us define too as three dimensional points (3D) the hand landmarks position referenced from the camera frame as $p_{Hlm^i}^c = [x_{Hlm^i}^c, y_{Hlm^i}^c, z_{Hlm^i}^c]$, where $i = 1 : n_i$. To find the relationship between p_{lm^i} and $p_{Hlm^i}^c$, the classic pinhole model equations (5, 6) have been used:

$$x_{Hlm^i}^c = (x_{lm^i} - u_0) z_{Hlm^i}^c / f \quad (5)$$

$$y_{Hlm^i}^c = (y_{lm^i} - v_0) z_{Hlm^i}^c / f \quad (6)$$

where u_0 and v_0 are the coordinates of the camera's principal point, f represents the camera's focal length, and $z_{Hlm^i}^c$ is the depth value. Generally, 3D vision sensors provide depth maps ($D \in \mathbb{R}^{w \times h}$) where, for each RGB pixel, there is an associated depth value for that pixel.

We will define the position vector of the wrist frame O_{wrist} coincident with the wrist landmark. Now, to obtain its orientation, let us define a new set of hand landmarks (p_{0_i}, with $i = 1 : n_i$). This set defines a new wrist frame ($\sum_{wrist'}$), which position vector is coincident with the wrist frame position vector O_{wrist}. The new set of hand landmarks is constant, and they have been chosen to make the orientation of $\sum_{wrist'}$ coincide with the robot frame orientation. Then, considering both sets of points p_{0_i} and p_{Hlm^i}, the rotation matrix between frames $\sum_{wrist'}$ and $\sum_{wrist}$ is calculated using the Horn algorithm [24], which provides the orientation vector φ_{wrist} of $\sum_{wrist}$ with respect to the robot frame.

Once the hand pose is calculated, the robotic manipulator EE, containing the detachable wristband, must perform a movement towards the approximation frame, which can be easily obtained with the transformation matrix presented in eq. (4). A control strategy is needed to continuously update the path ($\mathcal{P}_{EE}$) followed by the manipulator EE. A Model Predictive Controller (MPC) is an optimal control strategy based on numerical optimization methods. This controller

has been chosen due to its ability to handle constraints. In this case, the position and the velocity of the EE are constraint. Let us define the behavior of the EE as:

$$\boldsymbol{X}(t) = \begin{pmatrix} \boldsymbol{x_{EE}}(t) \\ \boldsymbol{v_{EE}}(t) \end{pmatrix}$$

$$\dot{\boldsymbol{X}} = f(\boldsymbol{X}(t), \boldsymbol{u}(t)) = \begin{pmatrix} \boldsymbol{v_{EE}}(t) \\ \boldsymbol{u} - \boldsymbol{v_{EE}} \end{pmatrix}$$

where $\boldsymbol{x_{EE}}(t)$, $\boldsymbol{v_{EE}}(t) \in \mathbb{R}^6$ represents the pose and velocity of the EE, respectively, and $\boldsymbol{u} \in \mathbb{R}^6$ is the control input. The MPC stabilizes a system according to its kinematics with a given reference by minimizing a cost function $g(\boldsymbol{X}(t), \boldsymbol{u}(t), r_i)$ subjected to some restrictions $h(\boldsymbol{X}(t), \boldsymbol{u}(t))$, being r_i the reference input, as shown in equations (7):

$$\min_{\boldsymbol{X}(t), \boldsymbol{u}(t)} J = \int_0^T g(\boldsymbol{X}(t), \boldsymbol{u}(t), r_i, Q, R) dt \quad \text{(7a)}$$

$$\text{s.t.} \quad \boldsymbol{X}(0) = \boldsymbol{X_{init}} \quad \text{(7b)}$$

$$\dot{\boldsymbol{X}}(t) = f(\boldsymbol{X}(t), \boldsymbol{u}(t)) \quad \text{(7c)}$$

$$h(\boldsymbol{X}(t), \boldsymbol{u}(t)) \leq 0 \quad \text{(7d)}$$

The system is discretized into N steps over a horizon T of size $dt = T/N$, and the cost function is defined as:

$$g(\boldsymbol{X}(t), \boldsymbol{u}(t), r_i, Q, R) = \|\boldsymbol{x_{EE}} - \boldsymbol{x_{approx}}\|_Q^2 + \|\boldsymbol{u_{k+1}} - \boldsymbol{u_k}\|_R^2 \quad \text{(8)}$$

being Q and R weight parameters and $\boldsymbol{x_{approx}} \in \mathbb{R}^6$ the pose of the approximation frame with respect to the robot frame. The problem is solved using a 4 order Runge–Kutta integrator $\boldsymbol{X_{k+1}} = \mathbf{f}_{RK4}(\boldsymbol{X_k}, \boldsymbol{u_k}, dt)$ subject to the aforementioned position and velocity EE constraints: $x_{EE}^{min} < x_{EE}^k < x_{EE}^{max}$ and $u^{min} < u^k < u^{max}$, respectively.

The visual moving hand tracking phase will end once two statements are achieved simultaneously for a specific period of time. We will define these two statements as detachable conditions. The first condition is achieved whenever the victim is ready and comfortable, thus maintains the hand pose constant. Consequently, the wrist frame $\sum_{wrist}$ will not vary in a predefined threshold. The second condition is triggered similarly to the first condition but with the EE frame $\sum_{EE}$ considered.

B. Haptic Force-controlled Detachable Wristband Placement

When the detachable conditions are triggered, we can assume the frames $\sum_{approx}$ and $\sum_{EE}$ are coincident. Therefore, the robotic manipulator EE is oriented to the victim's forearm, and the distance between the wristband and the forearm is d_z. A linear haptic force-controlled movement in the z_{EE} axis towards the victim's arm is conducted with a constant orientation. The movement is performed until the EE exerts the detachable force F_d previously calculated in eq. (1) for a specific period of time. This period must be sufficiently large to change the wristband from state I

TABLE I
PARAMETER VALUES OF THE DESIGNED WRISTBAND.

Parameter	ε	δ	K_s	x_0	θ_0
Value	0.8	$60°$	200 N/m	32 mm	$61.25°$

to state III, which gets the wristband placed around the victim's forearm. The arm of the victim is supposed to remain in the same position during the whole process. For a precise reading of the sensors the wristband is equipped with, it must be mounted in this particular manner. The haptic force-controlled detachable wristband placement phase ends whenever the wristband has been successfully placed. Once both phases have been carried out, the manipulator moves to a transport position, where it is coupled to the mobile robot.

V. EXPERIMENTAL SETUP

This section relates the materials and software utilized to follow the method scheme. The detachable wristband has been designed and built using additive manufacturing technology. In table I, the main parameters of the proposed wristband are presented. Different sensors are embedded in the detachable wristband: A pulse-oximeter sensor MAX30102 (Maxim Integrated, USA), a 9-axis inertial measurement unit MPU9250 (Invesense, USA), and a GPS module ublox NEO 6M (u-blox, Sweeden). An ESP-32 microcontroller based development board, the Heltec WIFI LoRa 32 V2 (Heltec, China), serves as the wristband's brain. An RGB-Depth camera is used for the 3D vision system, particularly the Intel RealSense D435 Depth Camera, which works properly in outdoor environments. The ROS wrapper realsense-ros version 2.3 has been used to obtain the camera depth and raw images. To improve the depth image quality and to reduce the noise levels, the spatial edge-preserving and the temporal filters have been implemented. These filters are also provided by realsense-ros wrapper.

For the moving hand tracking solution, *MediaPipe* [21] has been chosen. Three of the hand landmarks provided are used to approximate the palm plane (0, 5, and 17). The Horn algorithm is computed using python scripts and a ROS topic of the type "Pose" is used to publish the hand pose, at a rate of 100 Hz. An Extended Kalman Filter (EFK) is also implemented with the robot_localization 3.3.0 version ROS package to filter the hand pose noise.

The robotic manipulator used in the experiments is the KUKA LBR iiwa 7 R800. This manipulator is chosen due to its large workspace, capacity to detect external forces, and large payload. The KUKA Sunrise ToolBox [25] is used to effectively control the EE pose, while the trajectory is defined by the MPC in a control loop implemented in *Matlab*, using an Intel Core i7 8700K computer with 8 GB of RAM. The mobile robot is a commercial all-terrain platform Argo J8 Rover. This is an amphibious vehicle with a top speed of 16 km/h, a payload of 680 kg, 6 hours of full autonomy with eight low pressure tires for optimal performance in rough terrain scenarios, and can be tele-operated with a gamepad wired controller. Furthermore, the Rover is equipped with

Fig. 5. Consecutive frames (from top to bottom and left to right) of the RGB camera with the MediaPipe solution represented in experiment I. The hand pose changes in different directions and angles whilst the KUKA EE tracks it. Finally, the wristband gets placed around the forearm.

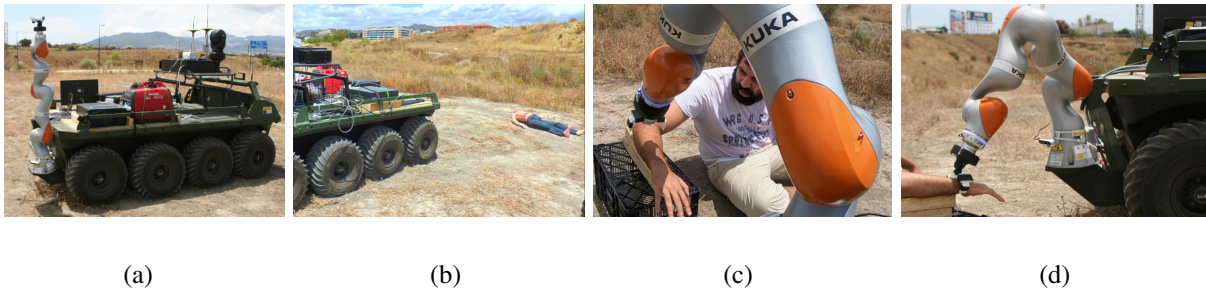(a)   (b)   (c)   (d)

Fig. 6. In (a), the mobile manipulator used in experiment II. In (b), the mobile manipulator performs the approximation to the victim, then in (c) the visual moving hand tracking phase is presented, followed by the haptic force interaction phase showed in (d).

different sensors to help with the tele-operation phase: A 3D-Lidar sensor (Velodyne HDL-32), an RGB, and TIR camera (Oculus-TI camera), and a GPS with RTK (JAVAD L1-band).

A quadratic optimization problem using a multi-shooting scheme is constructed to solve the discretized equations of (7) as a Sequential Quadratic Program (SQP). The system is discretized with $N = 20$ over a time horizon $T = 4$ s. $Q, R \in \mathbb{R}^{6 \times 6}$ are diagonal matrices defined as: $Q = diag(1, 1, 1, 8, 8, 8)$ and $R = diag(50, 50, 50, 50, 50, 50)$. The MPC solver uses an Interior Point Optimizer (IPOpt) algorithm, implemented with the CASADI software framework [26].

VI. Experiments

Two experiments have been carried out. The first one is made in the laboratory, with the whole system performing the detachable wristband placement procedure in a human, as seen in Fig. 5. The second experiment consists of a similar approximation, however, the manipulator is located in an all-terrain mobile robot (Fig. 6 (a)), and the person is lying on the floor in a SAR scenario. Both experiments have been recorded in video [1].

A. Experiment I. Laboratory Approach

A first laboratory approach is considered, with the KUKA located on the edge of a table. This experiment has been performed to prove the feasibility of the whole method. The final wristband placement procedure also validates the design

[1] https://youtu.be/EEp7yJtebJY

of the detachable wristband. The experiment consists of a hand in a non-stationary state, realizing movements while changing the palm orientation. The KUKA EE is supposed to track the hand pose, validating the visual moving hand tracking phase. For simplicity, the hand pitch angle is made constant ($\beta = 330°$). Once the detachable conditions have been triggered, the hand tracking stops, and the manipulator places the wristband around the forearm. The forces exerted by the EE are recorded to validate the haptic force-controlled detachable wristband placement phase.

B. Experiment II. Search-and-Rescue Scenario

In this experiment, the viability of the method in a SAR scenario is being analyzed. This experiment was part of a large scale disaster exercise held in Málaga on June 18, 2021. The scenario belongs to the University of Málaga, has $90\,000\,\mathrm{m}^2$, and is located next to our lab, in the campus. The area is a natural zone with multiple terrain altitudes, tunnels, and natural vegetation. Depending on the weather, a SAR scenario may have different illumination conditions. The experiment was performed on a sunny day, and the camera was not directly exposed to the sun.

As seen in Fig. 6 (b), the approximation of the mobile manipulator to the victim is carried out with the help of the various sensors mounted on the Argo and the Intel realsense D435 camera. Once the Argo is in position, the KUKA deploys, and the moving hand tracking phase begins, considering the all-terrain mobile manipulator is located in a place with no gradient since we want to avoid a
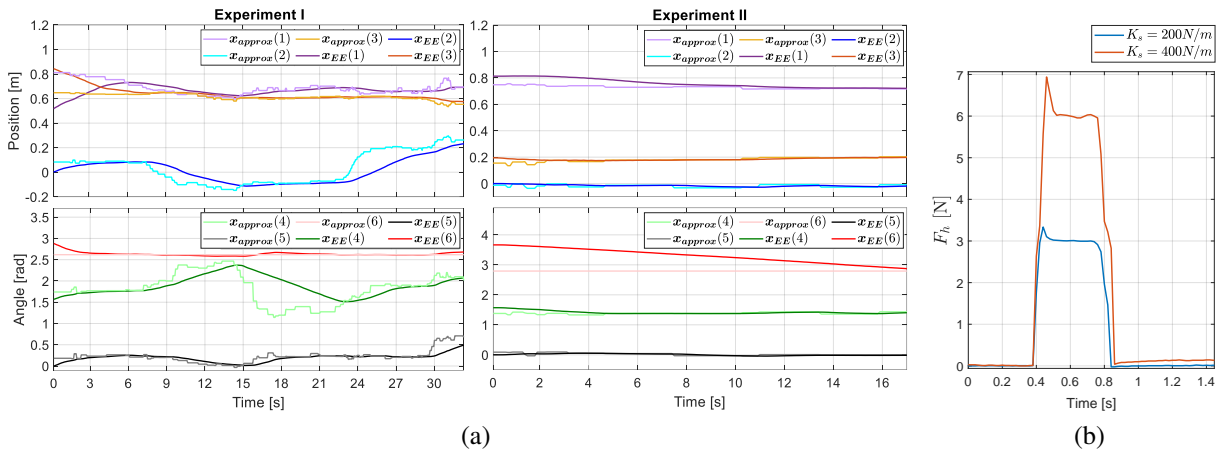
Fig. 7. In (a), the cartesian position (top) and orientation (bottom) of the robot EE ($\boldsymbol{x_{EE}}$) and the approximation frame ($\boldsymbol{x_{approx}}$) in the experiments I (left) and II (right). The force exerted (F_h) by the KUKA's EE in the wristband placement process is shown in (b), recorded with two springs with a different elastic constant.

malfunction of the gravity compensation mechanism of the KUKA manipulator. A similar approach to the one performed in experiment I is taken into consideration, but, in this case, as seen in Fig. 6 (c), the victim is sitting on the ground, with the hand in a semi-stationary state, resting on remains typical of a rescue scene.

Once the detachable conditions are triggered, the hand tracking stops, and the haptic force-controlled phase begins, as seen in Fig. 6 (d). Finally, the KUKA manipulator is moved to its transport position, and the mobile manipulator can be tele-operated to the next victim.

VII. RESULTS AND DISCUSSION

In Fig. 7 (a), the pose of the KUKA EE and the approximation pose are presented for each experiment. The columns represent both of the experiments, where the left-hand column is experiment I, and the right-hand column is experiment II. On the other hand, the top row represents the cartesian position and the bot row the cartesian orientation, both of them with respect to the robot frame. The data represented is $\boldsymbol{x_{approx}}$ (light colors) which indicates the information the 3D vision system provides about the approximation frame pose, and $\boldsymbol{x_{EE}}$ (dark colors), which shows the pose followed by the EE.

The performance is evaluated by comparing $\boldsymbol{x_{EE}}$ and $\boldsymbol{x_{approx}}$. Experiment I results show that the moving hand tracking is successfully performed, as the $\boldsymbol{x_{EE}}$ pose vector continuously adapts to the changes of $\boldsymbol{x_{approx}}$, reducing the error between both vectors. The wristband placement procedure is also successfully performed, as seen in the last three frames of Fig. 5. This experiment has been performed with nine different configurations to determine with which poses the method performs more effectively. We will define three intervals of 30º each for the hand roll and yaw angles ($\boldsymbol{x_{hand}}(4)$ and $\boldsymbol{x_{hand}}(6)$ respectively), being the intervals [{-45 , -15}, {-15 , 15},{15 , 45}]. All possible combinations of intervals have been tested a total of 30 times, and each success rate of all configurations is presented in table II,

TABLE II
EXPERIMENT I RESULTS

roll \ yaw	{-45 , -15}	{-15 , 15}	{15 , 45}
{-45 , -15}	96.6%	100%	100%
{-15 , 15}	100%	100%	100%
{15 , 45}	90%	93.3%	96.6%

considering as a success the placement of the detachable wristband around the human forearm and as a failure the non-placement of the detachable wristband. The success rate of all experiments combined is 97.4%. Although the results are promising, some aspects affect the performance. On the one hand, hand landmarks are calculated using a Neural Network based approach, which may find a solution with errors. In addition, the Intel realsense D435 camera has an RMS error in the z-axis of the camera frame.

On the other hand, the transformation matrix $\mathbf{T}_c^{robot}$ may be inaccurate, considering that some vibrations are produced once the KUKA is moving, affecting the pose of the camera frame. Therefore, with all these drawbacks, the final approximation frame calculated may not have the pose it should be, resulting in the force exerted by the EE is not perpendicular to the forearm; hence the process of getting the wristband placed is unsuccessful.

In Fig. 7 (b), the interaction force between the KUKA's EE and the forearm in a successful haptic force-controlled detachable wristband placement phase is presented. Two configurations of the wristband are analyzed. Both of them are parametrized with the values of table I, but with different springs, with two elastic constants ($K_s = \{200, 400\}N/m$). The corresponding value of F_d is calculated with eq. (1) and the force exerted is augmented by 20%, considering that there are frictional forces that must be overcome.

The method's feasibility in a SAR scenario has been evaluated in experiment II. As seen in Fig. 6, the Argo rover is capable of reaching with the KUKA manipulator attached, from a base station to a victim's location, through

rough terrain. Furthermore, the process is carried out without damaging it due to its location behind the Argo wheels. Then, the tracking of the hand pose is successfully performed (Fig. 7 (a)) as the EE gets to the approximation pose, where the haptic force-controlled detachable wristband placement phase is carried out successfully. As a result, we conclude that the method is viable in a SAR scenario, but with some limitations. The vision sensor needs minimum illumination conditions to obtain hand landmarks efficiently. Besides, the victim's hand needs to be in the workspace of the robotic manipulator. Therefore, getting the sensorized wristband placed will depend on the size of the robotic manipulator workspace, its position in the mobile robot, and the distance between the victim and the mobile robot.

VIII. Conclusions

This paper presented the design of a novel sensorized detachable wristband and the method for its placement to a victim in a SAR scenario. The approach to the victim was carried out with a mobile manipulator. The hand pose of the victim was calculated by a 3D vision system, while an MPC tracked its pose with the robotic manipulator EE. Finally, a haptic force-controlled movement was able to get the detachable wristband placed around the victim's forearm. Two experiments were conducted to prove the method's effectiveness in a laboratory and in a SAR scenario. The results presented in this letter showed the good performance of the designed detachable wristband and the proposed method in a SAR scenario.

Future research shall consider the limitation of the victim to be located in a place with no gradient with the addition of a tilting platform in the robotic manipulator's base. A similar approximation with the 3D camera bracket could be considered so that the camera could track the victim's moving hand more efficiently. In case of low vision environments, new hand landmarks detection methods, based on non-RGB images, will be taken into consideration to improve the capabilities of the whole system. Furthermore, the addition of 3D cameras to fuse the hand pose and enhance the information shall be considered.

References

[1] "World disasters report 2015," International Federation of Red Cross and Red Crescent Societies, 2015.

[2] P. A. O'Neill, "The abc's of disaster response," *Scandinavian journal of surgery*, vol. 94, no. 4, pp. 259–266, 2005.

[3] Y. M. Barilan, M. Brusa, and P. Halperin, "Triage in disaster medicine: ethical strategies in various scenarios," in *Disaster bioethics: Normative issues when nothing is normal*. Springer, 2014, pp. 49–63.

[4] T. Gao, T. Massey, L. Selavo, D. Crawford, B.-r. Chen, K. Lorincz, V. Shnayder, L. Hauenstein, F. Dabiri, J. Jeng, *et al.*, "The advanced health and disaster aid network: A light-weight wireless medical system for triage," *IEEE Transactions on biomedical circuits and systems*, vol. 1, no. 3, pp. 203–216, 2007.

[5] T. Klingeberg and M. Schilling, "Mobile wearable device for long term monitoring of vital signs," *Computer methods and programs in biomedicine*, vol. 106, no. 2, pp. 89–96, 2012.

[6] J. Bravo-Arrabal, M. Toscano-Moreno, J. Fernandez-Lozano, A. Mandow, J. A. Gomez-Ruiz, and A. García-Cerezo, "The internet of cooperative agents architecture (x-ioca) for robots, hybrid sensor networks, and mec centers in complex environments: A search and rescue case study," *Sensors*, vol. 21, no. 23, p. 7843, 2021.

[7] P. Escobedo, C. E. Ramos-Lorente, A. Martínez-Olmos, M. A. Carvajal, M. Ortega-Muñoz, I. de Orbe-Payá, F. Hernández-Mateo, F. Santoyo-González, L. F. Capitán-Vallvey, A. J. Palma, *et al.*, "Wireless wearable wristband for continuous sweat ph monitoring," *Sensors and Actuators B: Chemical*, vol. 327, p. 128948, 2021.

[8] B. Cvetković, R. Szeklicki, V. Janko, P. Lutomski, and M. Luštrek, "Real-time activity monitoring with a wristband and a smartphone," *Information Fusion*, vol. 43, pp. 77–93, 2018.

[9] R. R. Murphy, S. Tadokoro, and A. Kleiner, "Disaster robotics," in *Springer Handbook of Robotics*. Springer, 2016, pp. 1577–1604.

[10] M. K. Habib, Y. Baudoin, and F. Nagata, "Robotics for rescue and risky intervention," in *IECON 2011-37th Annual Conference of the IEEE Industrial Electronics Society*. IEEE, 2011, pp. 3305–3310.

[11] F. Niroui, K. Zhang, Z. Kashino, and G. Nejat, "Deep reinforcement learning robot for search and rescue applications: Exploration in unknown cluttered environments," *IEEE Robotics and Automation Letters*, vol. 4, no. 2, pp. 610–617, 2019.

[12] E. Price, G. Lawless, R. Ludwig, I. Martinovic, H. H. Bülthoff, M. J. Black, and A. Ahmad, "Deep neural network-based cooperative visual tracking through multiple micro aerial vehicles," *IEEE Robotics and Automation Letters*, vol. 3, no. 4, pp. 3193–3200, 2018.

[13] M. Atif, R. Ahmad, W. Ahmad, L. Zhao, and J. J. Rodrigues, "Uav-assisted wireless localization for search and rescue," *IEEE Systems Journal*, 2021.

[14] J. M. Gandarias, F. Pastor, A. J. Muñoz-Ramírez, A. J. García-Cerezo, and J. M. Gómez-de Gabriel, "Underactuated gripper with forearm roll estimation for human limbs manipulation in rescue robotics," in *2019 IEEE/RSJ International Conference on Intelligent Robots and Systems (IROS)*. IEEE, 2019, pp. 5937–5942.

[15] J. M. Gómez-de Gabriel, J. M. Gandarias, F. J. Pérez-Maldonado, F. J. García-Núñcz, E. J. Fernández-García, and A. J. García-Cerezo, "Methods for autonomous wristband placement with a search-and-rescue aerial manipulator," in *2018 IEEE/RSJ International Conference on Intelligent Robots and Systems (IROS)*. IEEE, 2018, pp. 7838–7844.

[16] A. Paolillo, K. Chappellet, A. Bolotnikova, and A. Kheddar, "Inter-linked visual tracking and robotic manipulation of articulated objects," *IEEE Robotics and Automation Letters*, vol. 3, no. 4, pp. 2746–2753, 2018.

[17] Y. Guo, F. Deligianni, X. Gu, and G.-Z. Yang, "3-d canonical pose estimation and abnormal gait recognition with a single rgb-d camera," *IEEE Robotics and Automation letters*, vol. 4, no. 4, pp. 3617–3624, 2019.

[18] A. Erol, G. Bebis, M. Nicolescu, R. D. Boyle, and X. Twombly, "Vision-based hand pose estimation: A review," *Computer Vision and Image Understanding*, vol. 108, no. 1-2, pp. 52–73, 2007.

[19] J. S. Supancic, G. Rogez, Y. Yang, J. Shotton, and D. Ramanan, "Depth-based hand pose estimation: data, methods, and challenges," in *Proceedings of the IEEE international conference on computer vision*, 2015, pp. 1868–1876.

[20] L. Ge, H. Liang, J. Yuan, and D. Thalmann, "Robust 3d hand pose estimation from single depth images using multi-view cnns," *IEEE Transactions on Image Processing*, vol. 27, no. 9, pp. 4422–4436, 2018.

[21] F. Zhang, V. Bazarevsky, A. Vakunov, A. Tkachenka, G. Sung, C.-L. Chang, and M. Grundmann, "Mediapipe hands: On-device real-time hand tracking," *arXiv preprint arXiv:2006.10214*, 2020.

[22] G. Du and P. Zhang, "A markerless human–robot interface using particle filter and kalman filter for dual robots," *IEEE Transactions on Industrial Electronics*, vol. 62, no. 4, pp. 2257–2264, 2014.

[23] S. E. Ovur, H. Su, W. Qi, E. De Momi, and G. Ferrigno, "Novel adaptive sensor fusion methodology for hand pose estimation with multileap motion," *IEEE Transactions on Instrumentation and Measurement*, vol. 70, pp. 1–8, 2021.

[24] B. K. Horn, "Closed-form solution of absolute orientation using unit quaternions," *Josa a*, vol. 4, no. 4, pp. 629–642, 1987.

[25] M. Safeea and P. Neto, "Kuka sunrise toolbox: Interfacing collaborative robots with matlab," *IEEE Robotics & Automation Magazine*, vol. 26, no. 1, pp. 91–96, 2018.

[26] J. A. Andersson, J. Gillis, G. Horn, J. B. Rawlings, and M. Diehl, "Casadi: a software framework for nonlinear optimization and optimal control," *Mathematical Programming Computation*, vol. 11, no. 1, pp. 1–36, 2019.